



Continuous gradient temperature Raman spectroscopy of N-6DPA and DHA from -100 to 20°C



C. Leigh Broadhurst^{a,b,*}, Walter F. Schmidt^a, Moon S. Kim^a, Julie K. Nguyen^a, Jianwei Qin^a, Kuanglin Chao^a, Gary L. Bauchan^c, Daniel R. Shelton^a

^a Environmental Microbiology and Food Safety Laboratory, U.S. Department of Agriculture Agricultural Research Service, 10300 Baltimore Avenue, Beltsville, MD 20705, United States

^b Department of Nutrition and Food Science, University of Maryland, College Park, MD 20742, United States

^c Electron and Confocal Microscopy Unit, Plant Sciences Institute, USDA ARS, Beltsville, United States

ARTICLE INFO

Article history:

Received 29 April 2016

Received in revised form 10 June 2016

Accepted 11 June 2016

Available online 18 June 2016

Keywords:

Gradient temperature Raman spectroscopy

n-6DPA

DHA

n-6 Docosapentaenoic acid

Docosahexaenoic acid

Raman spectroscopy

ABSTRACT

One of the great unanswered questions with respect to biological science in general is the absolute necessity of docosahexaenoic acid (DHA, 22:6n-3) in fast signal processing tissues. N-6 docosapentaenoic acid (n-6DPA, 22:5n-6), with just one less double bond, group, is fairly abundant in terrestrial food chains yet cannot substitute for DHA. Gradient temperature Raman spectroscopy (GTRS) applies the temperature gradients utilized in differential scanning calorimetry (DSC) to Raman spectroscopy, providing a straightforward technique to identify molecular rearrangements that occur near and at phase transitions. Herein we apply GTRS and DSC to n-6DPA and DHA from -100 to 20°C . 20 Mb three-dimensional data arrays with 0.2°C increments and first/second derivatives allowed complete assignment of solid, liquid and transition state vibrational modes, including low intensity/frequency vibrations that cannot be readily analyzed with conventional Raman. N-6DPA and DHA show significant spectral changes with premelting (-33 and -60°C , respectively) and melting (-27 and -44°C , respectively). The $\text{CH}_2-(\text{HC}=\text{CH})-\text{CH}_2$ moieties are not identical in the second half of the DHA and DPA structures. DPA has bending (1450 cm^{-1}) over almost the entire temperature range. In contrast, DHA contains major CH_2 twisting (1265 cm^{-1}) with no noticeable CH_2 bending, consistent with a flat helical structure with a small pitch. Further modeling of neuronal membrane phospholipids must take into account torsion present in the DHA structure, which essential in determining whether the lipid chain is configured more parallel or perpendicular to the hydrophilic head group.

© 2016 Published by Elsevier Ireland Ltd.

1. Introduction

One of the greatest challenges with respect to not only lipid physical chemistry but to biological science in general is the absolute necessity of DHA in fast signal processing tissues such as neuronal, retinal and cardiac. Over 600 million years of evolution the difference of just a single double bond has not been overcome: DHA is exclusively utilized from the diatom photoreceptor to the cephalopod eye to the primate brain (Gawrisch and Soubias, 2008;

Mitchell et al., 2012; Crawford et al., 2013, 2014; Janssen and Kiliaan, 2014; Brenna and Carlson, 2014). The severe neural and visual functional deficits which arise from the replacement of DHA with either n-3 or n-6DPA indicate that significant structural changes to lipid bilayers must occur, but only recently have such changes been quantified. DHA in the lipid bilayer is highly flexible and adaptable compared to saturated or monounsaturated fatty acids, converting between conformations in less than 100 ps (Gawrisch and Soubias, 2008). DHA's flexibility along with its extended homoallylic structure may allow DHA to closely follow the groove of the α -helix in G-coupled protein receptors (Feller et al., 2003; Kachlishvili and Brenna, 2013).

With extreme n-3 polyunsaturated fatty acid deprivation, n-6DPA may be incorporated into neural and retinal tissues leading to developmental disorders, neurodegeneration, dementia, memory loss, subnormal retinal signaling and loss of visual acuity (Moriguchi et al., 2004; Niu et al., 2004; SanGiovanni and Chew,

Abbreviations: CCD, charge coupled device; DHA, docosahexaenoic acid; n-6DPA, n-6 docosapentaenoic acid; DSC, differential scanning calorimetry; GTRS, gradient temperature Raman spectroscopy.

* Corresponding author at: Environmental Microbiology and Food Safety Laboratory, Bldg. 161 Rm. 116, U.S. Department of Agriculture Agricultural Research Service, 10300 Baltimore Avenue, Beltsville, MD 20705, United States.

E-mail address: leigh.broadhurst@ars.usda.gov (C. L. Broadhurst).

2005; Dyall and Michael-Titus, 2008). N-6DPA is also highly flexible and adaptable, however isomerization rates for DHA are faster, especially at the methyl end (Eldho et al., 2003; Gawrisch and Soubias, 2008). Within the lipid bilayer, DHA tends to concentrate near the water-lipid interface while n-6DPA does not (Eldho et al., 2003; Gawrisch and Soubias, 2008). In phosphatidylcholine membranes, n-6DPA and to a slightly lesser extent n-3 DPA acyl chain packing is less disordered in the midplane compared to packing of DHA chains. The 18:0, 22:6n-3 packing is considerably less constrained than the packing of 18:0, 22:5n-6, again highlighting the extreme flexibility and adaptability of DHA (Eldho et al., 2003; Mitchell et al., 2012).

In normal retinal rod outer segments 40–50% of the phospholipid fatty acids are DHA. Near-stoichiometric substitution of n-6DPA for DHA in rat rod outer segment membranes resulted in a 3-fold reduction cGMP phosphodiesterase activity, which ultimately delayed retinal signaling by 31 ms (Niu et al., 2004). Likewise, n-6DPA substitution in bovine rod outer segments reduced cGMP phosphodiesterase activity 2-fold, but n-3DPA substitution did not significantly affect this step in visual signal transduction. At physiological temperatures, both DPAs reduced the concentration of activated rhodopsin (MII) formed but the reduction was significantly greater for n-6DPA. Overall, results agree that the n-6 bond position is the most important factor in loss of visual function (Mitchell et al., 2012).

Enzyme systematics are also affected by the substitution of DPA for DHA. In syntheses of LC-PUFA-rich structured lipids from high laurate canola oil, eicosapentaenoic acid and DHA were preferentially incorporated into *sn*1,2 positions but n-3DPA was incorporated randomly (Hamam and Shahidi, 2006). Akanbi et al. (2014) found that pancreatic lipase selectively hydrolyzes n-3DPA over eicosapentaenoic acid and DHA, based on DPA's lack of double bonds close to the carbonyl group (initial bond at Δ 7) rather than its position on the glycerol backbone. Note this structural difference would not apply to n-6DPA, with an initial double bond at Δ 4.

On the other hand, both DPAs are components of many natural foods, n-3 primarily in the marine food chain and n-6 in the terrestrial, so also have positive health attributes. Like the more familiar marine lipid components eicosapentaenoic acid and DHA, increased levels of n-3DPA are associated with reduced platelet aggregation, chronic inflammation, c-reactive protein and triglycerides (Kaur et al., 2011; Byelashov et al., 2015; Dyall, 2015; Skulas-Ray et al., 2015). Limited animal research indicates that n-6DPA acts similarly (Nauroth et al., 2010; Chen et al., 2012).

A more complete understanding of DPA physical chemistry and biochemistry requires considerably more basic analytical data on these molecules than is currently available. However, fully elucidating the structures of the various long chain polyunsaturated fatty acids *via* infrared or Raman spectroscopy has been a daunting task due to the repetitive nature of the acyl/olefin chains and drastic decreases in melting points as the number of double bonds increases. Consequently only the vibrational modes of oleic acid (18:1n-9) and linoleic acid (18:2n-3), have been fully characterized over a range of temperatures (Mishra et al., 2010; Pi et al., 2011; Unger et al., 2013; Broadhurst et al., 2015).

Recently we presented the first complete and interpreted Raman spectrum of linoleic acid (Broadhurst et al., 2015) utilizing a technique we developed, continuous gradient temperature Raman spectroscopy (GTRS) (Qin et al., 2010; Schmidt et al., 2015a,b). GTRS applies the precise temperature gradients utilized in differential scanning calorimetry (DSC) to Raman spectroscopy. DSC is a powerful technique that quantifies heat absorption of molecules, providing information regarding phase transitions and fundamental thermodynamic properties, but not on the mechanisms by which heat is absorbed at the molecular level. GTRS correlates

Raman frequency shifts in solid or liquid samples with the specific temperature ranges in which elastic molecular structures absorb heat. We can easily detect changes that occur in less than 1 °C temperature increments; more precise measurements can be made utilizing shallower gradients over specific temperature ranges of interest. Thus, GTRS provides a very rapid and straightforward technique to identify theoretically proposed molecular rearrangements that occur just prior to or at phase transitions. In the temperature range of a transition between two stable forms of a compound, GTRS can identify the temperature at which steady state conditions are perturbed, and non-steady state vibrational modes specific to the transition state can be identified. GTRS provides far more data in far less time than conventional Raman at room temperature or with incremental temperature steps.

In this contribution we extend the GTRS technique from cryogenic to warm liquid temperatures for n-6DPA and DHA. A complete set of Raman frequencies and intensities vs. temperature are reported with conventional spectra and three-dimensional contour plots, and correlated with DSC data. Based on the complete spectra, molecular structures for both molecules are proposed that clearly differentiate their solid state structures, and indicate that DHA is a flat helical structure with small pitch, due to a similar direction of torsion/twist among the six double bonds. A second publication will cover n-3DPA.

2. Materials and methods

The GTRS system utilizes a 785-nm laser module (I0785MM0350MF-NL, Innovative Photonic Solutions, Monmouth Junction, NJ) as the excitation source. A fiber optic Raman probe (RPB, InPhotonics, Norwood, MA) is used to focus the laser and acquire the Raman signals. A bifurcated fiber bundle with a 16-bit CCD camera (1024 × 256 pixels; Newton DU920N-BR-DD, Andor Technology, South Windsor, CT) delivers the laser radiation to the probe and transmits the Raman signals to the spectrometer at 0.2 °C increments. The spectrometer detects a Raman shift range of 102.2–2538.1 cm^{-1} with a minimum spectral resolution of 3.7 cm^{-1} .

N-6DPA (*cis*-4,7,10,13,16 docosapentaenoic acid) 98% purity was purchased from Santa Cruz Biotechnology, Dallas, TX. DHA (*cis*-4,7,10,13,16,19 docosahexaenoic acid) >99% purity was purchased from Sigma Chemical Co., St. Louis, MO (Fig. 1). Materials were stored frozen in break-seal containers until immediately prior to use. Upon opening, 5 mg samples were pipetted within seconds directly onto aluminum pans which are inset on a 350 g copper heat sink. The heat sink and sample pan are prechilled in a liquid N₂ bath, so the sample reaches cryogenic temperatures almost instantaneously and is completely surrounded by nitrogen vapor during the transfer. We found no evidence for sample oxidation with this rapid, cold procedure. The sample itself does not come in direct contact with liquid N₂ or atmospheric water vapor condensate.

A ceramic hotplate is used for controlled heating of samples and as stable insulating platform for analysis. The copper heat sinks are placed directly on the ceramic heat surface or in a small liquid nitrogen bath on the hotplate, and serve to buffer the rate of temperature increase. Two K-type thermocouple probes are attached to two sides of the sample area and connected to a dual-input thermometer (EasyView EA15, Exttech Instruments, Nashua, NH). The sample temperature is defined as the average value of the two probes. The Raman probe, hotplate, and sample materials are placed in a closed black box to avoid ambient light. The sample box has a continuous flow of dry N₂ to minimize oxidation from atmospheric oxygen and water vapor. Raman spectra can be acquired from –180 to 320 °C. The heating gradient was approximately 1 °C min⁻¹ for these mainly cryogenic investigations. We did not use a set time schedule for spectral acquisition, but rather acquired

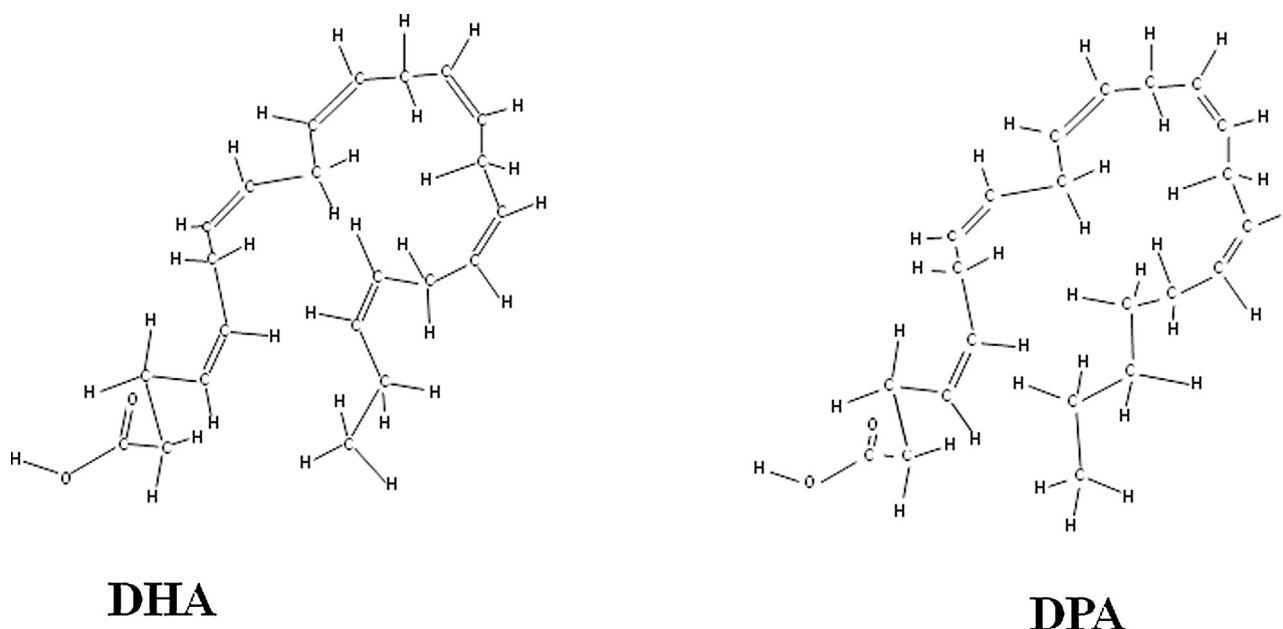


Fig. 1. DHA and n-6DPA structures.

spectra each time the sample temperature increased either 1 °C or 0.2 °C, depending on the analysis. System software was developed using LabVIEW (National Instruments, Austin, TX) to fulfil functions such as camera control, data acquisition, temperature measurement, and synchronization (Qin et al., 2010). All samples were run in triplicate with fresh material utilized for each run to avoid problems with oxidation and sample evaporation, and each dataset analyzed independently to ensure reproducibility.

SigmaPlot 13 (Systat Software, Inc.) generated three-dimensional contour plots (frequency, temperature, signal intensity). First derivative intensity contour plots were calculated using a three-point running average, *i.e.* the first and last points calculate the slope of the middle point. The contour plots for the second derivative intensity were calculated using the three-point running average data from the first derivative spectra. Relative intensity is scaled for the signal intensity range within each of the six spectral wavelength sets given. Maximum to minimum intensity colors are red > orange > yellow > green > blue > black. Each contour data array contains about 20 Mb.

For DSC data separate fresh 5 mg lipid sample equilibrated to 25 °C prior to unsealing were utilized. Under N₂ vapor, samples were pipetted into aluminum pans, crimp-sealed and placed in the instrument in seconds. We utilized a Q200 differential scanning calorimeter (TA Instruments, New Castle, DE) with heating rates of 10.0 °C and 1.0 °C min⁻¹ for DHA and 2.0 °C min⁻¹ and 0.5 °C min⁻¹ for n-6DPA from -95 °C to -10 °C. For DHA, specific areas that did not include the melt transition (-80 to -55 °C) were also focused on with 1.0 °C min⁻¹ and 0.5 °C min⁻¹ scans in order to capture relatively small changes in heat flow. Samples were scanned under a continuous N₂ flow heated at the same rate as the sample which also prevents sample oxidation. All samples were run in triplicate and each dataset analyzed independently to ensure reproducibility.

3. Results

For DHA at the 10.0 °C min⁻¹ heating rate, only a single sharp endothermic peak for melting was observed, starting at about

-50 °C with a sharp maximum at -44 °C (Fig. 2). At both the 1.0 min⁻¹ and 2.0 min⁻¹ heating rate, smaller endothermic peaks at -56 °C and -52 °C indicate solid state molecular rearrangements are occurring prior to the melt (Fig. 2 green curve). Concentration on the area -90 to -60 °C showed uniform heat flow; a small increase near -69 °C was not significant. For n-6DPA, only a single endothermic peak at -27 °C was observed at both heating rates.

Vibrational modes and assignments for n-6DPA and DHA are given in Table 1. Overall, sets of frequencies vary concurrent with the DSC phase data within low (cryogenic), intermediate (phase transitional), and high (above melting) temperature ranges for each fatty acid, so three/four ranges for have been utilized in Table 1 for ease of presentation, along with footnotes describing detailed temperature-dependent behavior. Fig. 3 shows representative line spectra for DHA; spectra at any temperature for either molecule available upon request.

Figs. 4 and 5 show spectral contour plots. Constant temperature Raman measurements contain perhaps 1 K of spectral data; GTRS easily generates several Mb of data in each array. A shallower gradient in which spectra are collected every 0.2 or 0.5 °C over a narrower range enables concentrating the sensitivity of the array to specific temperature ranges of interest. The contour plot easily distinguishes the temperature ranges over which vibrational mode patterns are constant, and when they begin to change.

4. Discussion

The contour plots for DHA and n-6DPA differ significantly than one for oleic acid that we generated previously (Broadhurst et al., 2015). With only a single a double bond, oleic acid has a clear solid state order-disorder phase transition at -4 °C, followed by the melt transition at 13 °C, in accordance with published phase equilibria and DSC data (Mishra et al., 2010; Pi et al., 2011; Unger et al., 2013). Our data showed that melting in the oleic acid molecule initiates at the double bond group (C9=C10) in the middle of the structure and moves outwards towards both ends of the molecule.

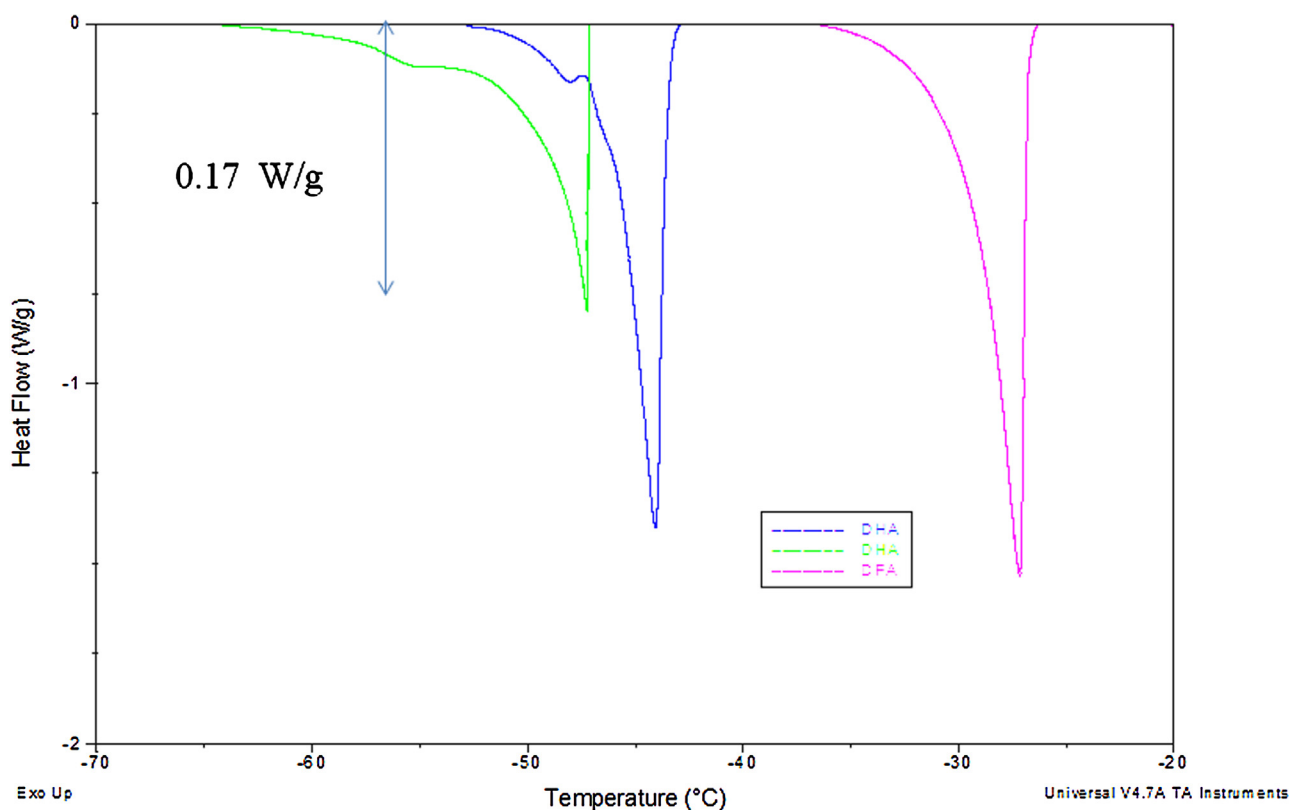


Fig. 2. Differential scanning calorimetry heat absorption data for DHA and n-6DPA; full scale data at $2^{\circ}\text{C min}^{-1}$. The strong endothermic peaks with maximum intensity at -44°C and -27°C respectively, correspond to melting and did not differ at $10^{\circ}\text{C min}^{-1}$. The green DHA curve is a larger scale (full scale 0.17 W/g) run for DHA at $1^{\circ}\text{C min}^{-1}$ that stops just prior to melting, showing the detail of smaller endothermic peaks at -56°C and -52°C which may be evidence for a solid state phase transition. (For interpretation of the references to colour in this figure legend, the reader is referred to the web version of this article.)

In contrast to oleic and linoleic acids (Ueno et al., 2000), no solid state phase transitions have been reported for DHA or DPA. Our DSC data do not reflect any such significant changes in heat flow other than perhaps a “premelting” type transition for DHA starting $\sim 15^{\circ}$ prior to melting (Fig. 2). X-ray diffraction analysis will be required to confirm if this is a solid state phase transition.

With a series of methylene groups, DHA and DPA melt at much lower temperatures than oleic and linoleic acids without such striking Raman frequency shifts. Previously, melting in LC-PUFA could only be explained with a model where all methylene groups or double bonds initiate melting simultaneously. However GTRS identifies the methylene group vibrations near the middle of their structure as the most elastic, and shows that the least elastic carbons are the ones nearest the carbonyl and methyl groups. In other words, the ends of the molecule are the “last” to melt.

It is understood that this work refers only to the free fatty acids and must be expanded to phospholipids and if possible membrane structures. The gel-fluid transition temperature for 1-stearoyl-2-docosahexaenoyl-*sn*-glycero-3-phosphocholine (18:0, 22:6n-3 PC) is more than 40°C higher than the DHA melting temperature. Thus the vibrational modes of DHA and n-6DPA in the warm solid or “premelting” region are almost certainly a better model for these long-chain fatty acids contained within the lipid bilayer than the vibrational modes of the 37°C liquids, which are close to or at isotropy. Further, it is plausible that the elastic molecular sites involved in the DHA and n-6DPA free fatty acid melt phase transition are the same sites of elasticity for these fatty acids contained within the lipid bilayer, but with the added constraints of the glycerophosphate head group this is not necessarily the case. A combination of GTRS with Raman and infrared techniques

developed for intact membrane analysis (Schultz 2011; Lewis and McElhane, 2013) is fairly straightforward and has great potential to yield novel results.

N-6DPA has significant conformational changes associated with premelting followed by melting initiating *circa* -33°C : (1) Above -33°C $\nu(\text{C}-\text{C})_{\text{sym}}$ and $\nu(\text{C}-\text{C})_{\text{asym}}$ are no longer predominant; (2) intensity at 965 cm^{-1} , 841 cm^{-1} and 406 cm^{-1} goes from weak to strong; (3) 929 cm^{-1} goes from strong to very strong; (4) a strong mode at 725 cm^{-1} shifts to 714 cm^{-1} ; (5) a strong mode at 579 cm^{-1} gradually becomes a weak mode at 596 cm^{-1} (Fig. 4). For oleic acid, density functional theory modeling (Mishra et al., 2010) assigns 596 cm^{-1} to $\delta(\text{CC9C}) + \delta(\text{CC10C}) + \delta(\text{C9}=\text{C10})$ and this frequency shift is associated with the initiation of melting. The molecular site in DPA that most closely corresponds to the $\delta(\text{CC9C}) + \delta(\text{CC10C}) + \delta(\text{C9}=\text{C10})$ OA structure is $\text{C16}=\text{C17}$, the aliphatic chain subsequent to the last double bond, with corresponding mode $\delta(\text{CC16C}) + \delta(\text{CC17C})$.

DHA also has significant conformational changes associated with premelting/melting initiating at -60°C : (1) Rocking at C15H2 *ca.* 725 cm^{-1} turns into CH wagging at that same site; (2) rocking at C12H2 near 862 cm^{-1} diminishes and shifts frequency (3) $\text{C}=\text{C11H}$ out of plane wagging plus $\text{HC13}=\text{C}$ out of plane wagging shift towards each other (frequencies become more equal); (4) C14H wagging at 716 cm^{-1} shifts slightly. Overall, the sites that can be considered “premelting” sites, or in other words—the sites that initiate changes just after -60°C —are within the elastic middle of the DHA structure. CH out-of-plane wagging at any given $\text{C}=\text{CH}$ site coincides with a disruption of CH_2 rocking at $\text{C}=\text{CH}-\text{CH}_2$ (or $\text{CH}_2-\text{HC}=\text{C}$) sites. Changes in CH_2 rocking near the middle of the

Table 1
Raman vibrational frequencies and spectral assignments. S: strong, M: moderate, W: weak.

DPA Temperature range (°C)			DHA Temperature range (°C)				Assignment
–100 to –78	–78 to –33	–33 to 0	–100 to –70	–70 to –62	–62 to –48	–48 to –20	
1660m	1661w	1659vs	1661s	1660s	1659s	1659s	$\nu(\text{C}-\text{C}_a) + \nu(\text{C}_a\text{C}_b) + \nu(\text{C}_b-\text{C}) + \rho(=\text{C}_b\text{H})_{\text{ip}} + \rho(\text{HC}_a)_{\text{ip}}$
1443w	1446w 1268w	1444w	–	–	–	–	$\delta(\text{CH}_2)^{\text{a}}$ $\gamma(\text{CH}_2)$ $\gamma(\text{CH}_2)$ $\gamma(\text{CH}_2)^{\text{b}}$
1262m		1264m	1265s	1265m		1261m	$\nu(\text{C}-\text{C})_{\text{asym}}$
			–	–	1072w	1072w	$\omega(\text{HC}=\text{C11H})_{\text{op}_{\text{sym}}}$
	977w		979m		1017w	1017w	$\omega(\text{H13C}=\text{CH})_{\text{op}_{\text{sym}}}$ $\omega(\text{HC}=\text{C11H})_{\text{op}_{\text{asym}}}$
968w		967s		972w ^c	972s	972s	$\omega(\text{H13C}=\text{CH})_{\text{op}_{\text{asym}}}$
928m	928m 883w	928m	927m	929w	926m	926m	$\omega(\text{H}_{16}\text{C}=\text{CH})_{\text{op}}$ and $\omega(\text{HC}=\text{C14H})_{\text{op}}$
			866m	863			$\omega(\text{HC}=\text{C17H})_{\text{op}_{\text{sym}}}$ $\omega(=\text{CH}-\text{C12}-\text{H}_a)_{\text{op}}$
841		840s			860s	860s	$\rho(\text{C12H}_2)^{\text{c}}$ $\omega(\text{HC}=\text{C17H})_{\text{op}_{\text{asym}}}$
	726s		727vs	724s			$\rho(\text{C15H}_2)^{\text{d,e}}$
719		716s 598w			722w	717	$\omega(=\text{CH}-\text{C15}-\text{H}_a)_{\text{op}}$ $\delta(\text{CC16C}) + \tau(\text{C16C17}) + \delta(\text{CC17C})$
584w	579s		581w		584vw		$\delta(\text{CC13C}) + \tau(\text{C13C14}) + \delta(\text{CC14C})^{\text{e}}$
	462vw		–	–	461	516w	$\delta(\text{C}-\text{C1O})$
407w		410s	406s	408w	408s	461s	$\delta(\text{CC3C})$
	395s				413s		$\delta(\text{CCC})$
			323s	322	322s	322s	$\delta(\text{O}=\text{C1}-\text{C}) + \delta(\text{CC3C})$
	314s						$\text{CC19C} + \tau(\text{C19C20})$
289		290s	289s		290s	288s	$\delta(\text{CC2C})$ $\text{CC16C} + \tau(\text{C16C17})$
239vw					239vw	239vw	$\tau(\text{C21}-\text{C22})$

Notes: DHA and DPA (n-6) are structurally identical from C1–C18. After C18 in DHA $-(\text{HC19}=\text{C20H})-\text{C21H}_2-\text{C22H}_3$ is present whereas in DPA $-\text{C19H}_2-\text{C20H}_2-\text{C21H}_2-\text{C22H}_3$ occurs. In DHA, for the repeating structural moieties $(\text{HC}=\text{CH})-\text{CH}_2-(\text{HC}=\text{CH})$, CH_2 occurs only at C6, C9, C12, C15, C18; C12H_2 is the middle one of this set of five. In DPA, C18H_2 does not occur and C15H_2 is the terminal one of this set of four. In DHA $\rho(\text{CH}_2)$ occurs at site C12, whereas in DPA $\rho(\text{CH}_2)$ occurs at site C15. When $(\text{HC}=\text{CH})-\text{CH}_2-(\text{HC}=\text{CH})$ site is not symmetrical, CH_2 will be CH_aH_b ; CH_2 rocking at that site becomes $=\text{CH}-\text{CH}_a$, $\text{H}_a\text{C}-\text{HC}=\text{}$ and/or $=\text{CH}-\text{CH}_b$ out-of-plane wagging.

^a CH_2 bending (ca. 1446 cm^{-1}) changes with temperature in DPA, not in DHA.

^b CH_2 twisting (ca. 1265 cm^{-1}) changes with temperature in both DPA and DHA.

^c C12H_2 rocking (860 cm^{-1}) is predominant in DHA, especially above -60°C .

^d C15H_2 rocking (726 cm^{-1}) is predominant in DHA, especially below -60°C .

^e Strong C15H_2 rocking in DPA is maximum intensity near -55°C ; concurrently maximum intensity for $\text{C}-\text{C}=\text{C}-\text{C15}$ in-plane bending (579 cm^{-1}) is observed.

lipid structures initiate conformational change, then this disruption of molecular order extends further into the lipid structure.

4.1. Three Dimensional Structures of DHA and n-6DPA

Just as the variables distance, velocity and acceleration cannot vary independent of one another, neither can curvature, torsion and torque. Distance requires two non-identical data points which generate a line. Curvature requires three data points (two non-colinear) to generate a plane. Torsion occurs from the addition of a fourth non-coplanar point above or below the plane of curvature. The direction above/below the plane of curvature can be unambiguously assigned as left-handed or right-handed. The direction of torque from out-of-plane torsion can always be discerned and will always be internally self-consistent.

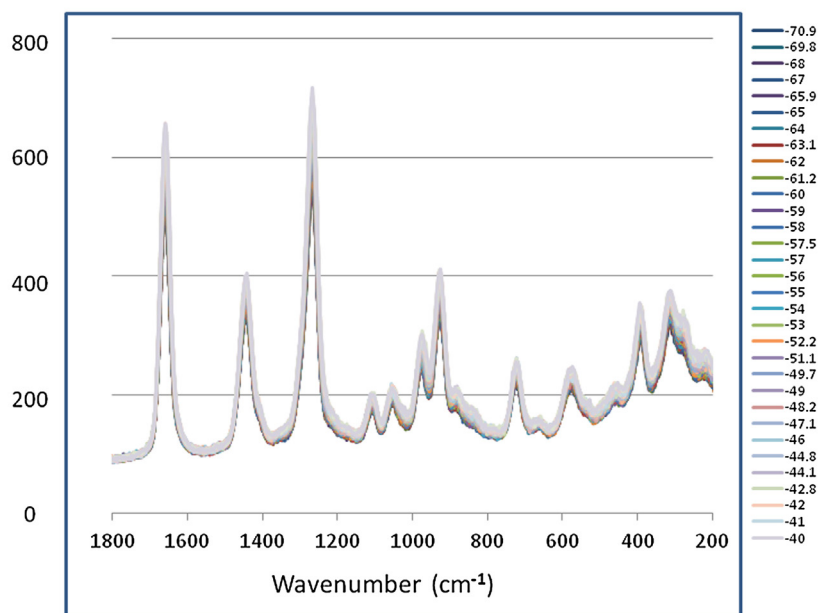
Vibrational mode assignments for structures that include at least four data points allow for three-dimensional structural interpretation of the spectral data. Further, four data points are prerequisite for asymmetry to be present. In-plane wagging is no different from in-plane bending, whereas out-of-plane wagging manifests torsion either above or below the plane. Without observing sets of at least four data points: (1) accounting of the relative direction of torsion from site to site is totally lost; (2) self-consistent three-dimensional structures remain undetectable; (3) local sites of molecular stress due to torsion are not identified, which precludes understanding of the torque components in

molecular order/disorder or folding/unfolding (Ogurtani, 2006, 2016).

Regardless of temperature, DHA has almost no Raman signal near 1450 cm^{-1} (CH_2 bending); the strong consistent signal near 1265 cm^{-1} is assigned to CH_2 twisting. Strong signals near 980 cm^{-1} , 920 cm^{-1} , and 860 cm^{-1} are assigned to $\text{C}-\text{C}=\text{C11}-\text{H}$ and $\text{C}-\text{C}=\text{C13}-\text{H}$ out-of plane wagging, and C12H_2 rocking respectively. Out-of-plane wagging at $\text{C11}-\text{H}$ and $\text{C13}-\text{H}$ differ by 60 cm^{-1} , therefore $\text{H}-\text{C11}-\text{C12}-\text{C13}$ vs. $\text{C11}-\text{C12}-\text{C13}-\text{H}$ are nonequivalent. Unequal $\text{C11}-\text{C12}$ versus $\text{C12}-\text{C13}$ stretching due to unequal torsion from $\text{C11}-\text{H}$ and $\text{C13}-\text{H}$ wagging is the most plausible explanation. A very intense mode near 1670 cm^{-1} indicates $\text{C}-\text{C}$ and $\text{C}=\text{C}$ stretching vibrational modes are very similar between sets of $\text{C}-\text{C}$ and $\text{C}=\text{C}$ pairs. Typically, single bond $\text{C}-\text{C}$ and double bond $\text{C}=\text{C}$ stretching bond lengths would be unequal. Signal near 1070 cm^{-1} above -60°C indicates asymmetrical $\text{C}-\text{C}$ stretching is present.

Conversely, the n-6DPA contour plot has strong signal at 1450 cm^{-1} over almost the entire temperature range, indicating CH_2 bending is occurring. Since CH_2 bending and CH_2 twisting are relative to the conformations of the adjacent planar $\text{HC}=\text{CH}$ sites, identifying the specific molecular sites at which bending occurs is not straightforward. However, lack of torsion at either end of the DPA molecule would result in bending at the third of five double bonds. Unlike DHA, DPA has an absence of signal ca. 1070 cm^{-1} which indicates that in $\text{C}=\text{C}-\text{C}_n-\text{C}=\text{C}$ sequences, $\text{C}-\text{C}_n$ and C_n-C stretching is not asymmetrical. Unexpectedly, two bond

A Overlay DHA Spectra from -70°C to -40°C at 1°C increments



B Overlay DHA Spectra from -40°C to -20°C in 1°C increments

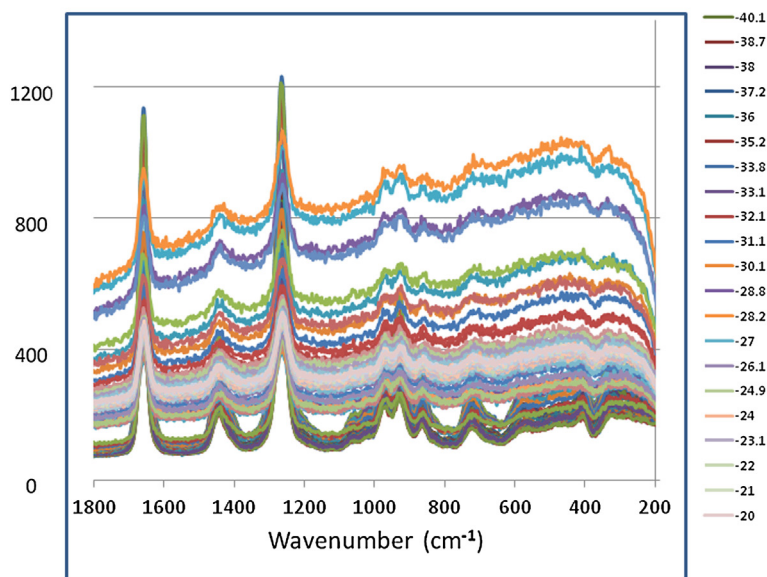


Fig. 3. Composite overlay line spectra for DHA showing some of the hundreds of spectra utilized to generate contour plots. Intensity scale is true: intensity is overall lower and less variable in the solid, and increases in both magnitude and variability in the premelting range. Just past the melt transition, liquid state spectra remain very similar as temperature increases and lack the spectral detail evident in the solid state spectra. (a) -70 to -40°C . (b) -40°C to -20°C . The highest intensity bright orange lines at -33.8°C , just beyond the melt phase transition. The next two highest intensities (green and orange) are -27.9°C and -28.8°C . (For interpretation of the references to colour in this figure legend, the reader is referred to the web version of this article.)

C—C symmetrical stretching vibrational modes in both n-6DPA and DHA are not observed; instead lower frequency C—C_n—C= three-atom bending in-plane bending is observed. In DPA, C—C_n—C= bending is particularly intense (red) near 580 cm^{-1} from -70°C to -33°C , and present, though less intense (green), outside that temperature range.

Molecular modeling (Hyperchem 8.0, Hypercube Inc., Gainesville, FL) independently supports our GTRS results. Although DHA and DPA are considered structural analogs, torsion needs not be

localized at the same molecular sites, and torsion can sum differently starting from the carbonyl vs. methyl ends, in agreement with previous authors (Gawrisch and Soubias, 2008) we found the two lipids are conformationally similar at only at the carbonyl end (Fig. 6). Tables 2a and 2b list the torsion angles in DHA and DPA for all sets of four carbon atoms containing a double bond. Torsion in DPA for C8—C9—C10=C11 and C10=C11—C12—C13 has similar intensity and direction (-148° vs. -157°), which structurally corresponds to symmetry about the

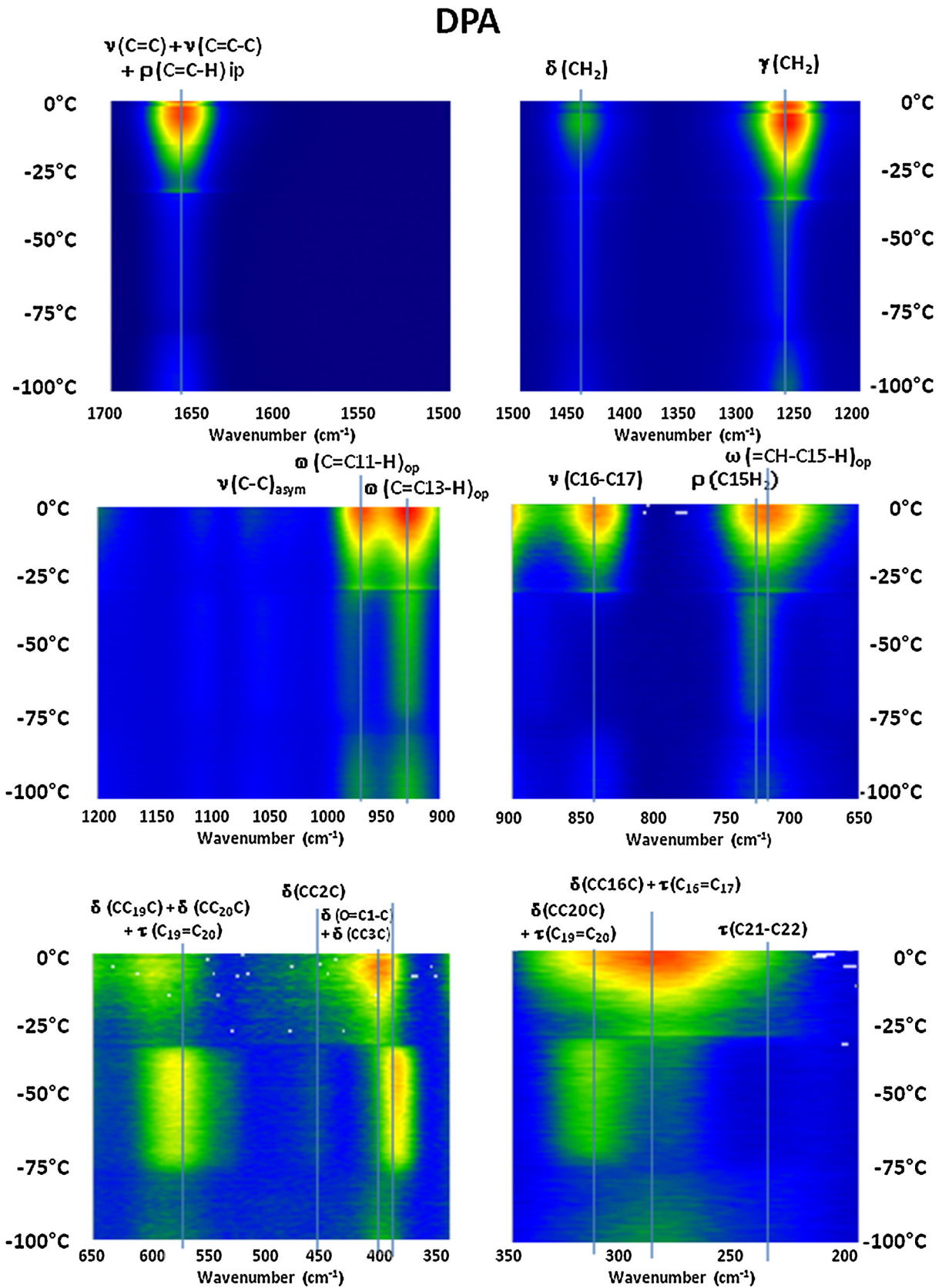


Fig. 4. Full scale gradient temperature Raman contour plot for n-6DPA. The melt transition (-27°C) appears as a discontinuity with respect to both intensity and frequency. Bending and twisting frequencies increase in intensity starting *circa* -75°C , and show the largest frequency shifts at melting. Beyond 0°C the spectrum increasingly broadens and then becomes isotropic.

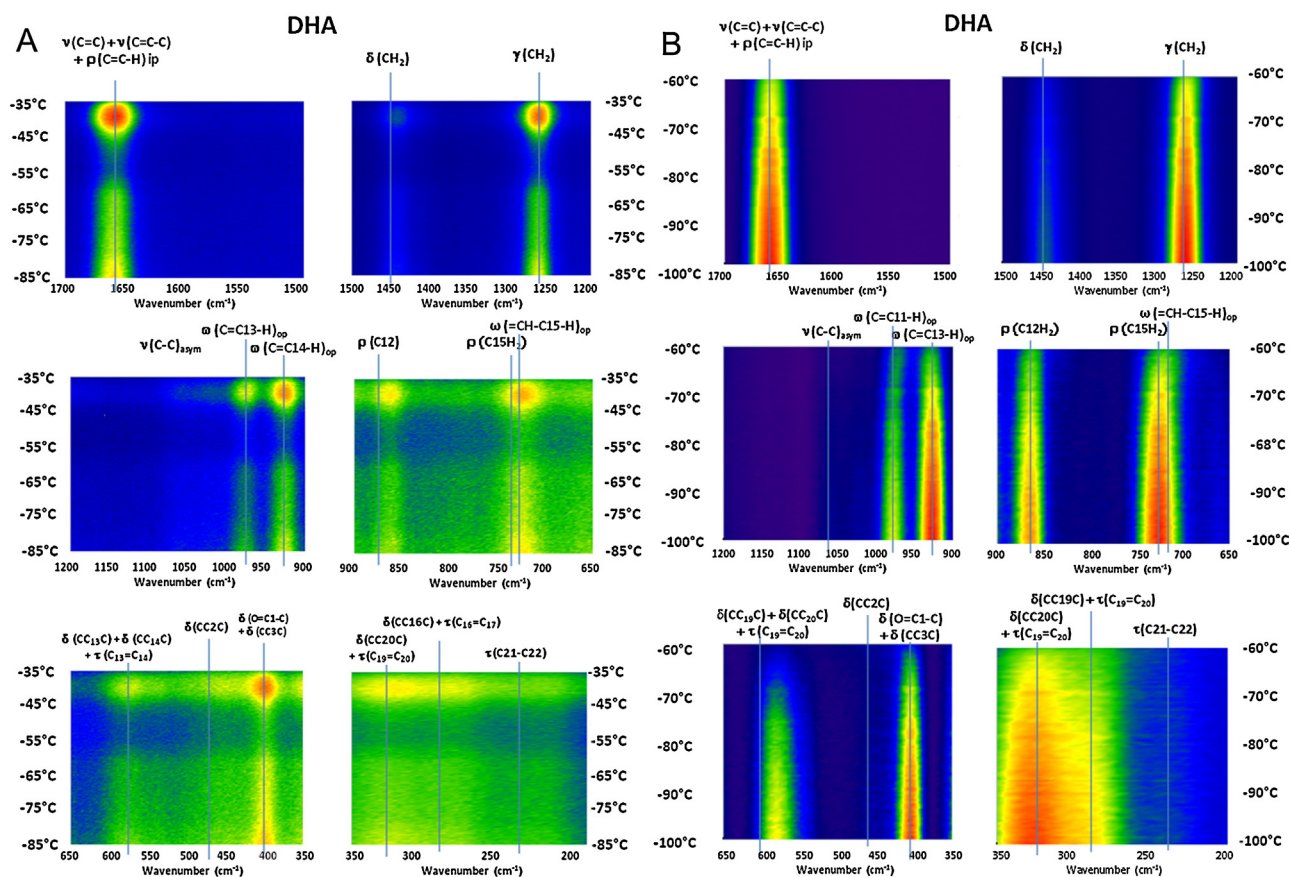


Fig. 5. (a) Full scale gradient temperature Raman contour plot for DHA. The melt transition (-44°C) has very little frequency shift. Prior to the melt there is an extended area starting at about -60°C with decreased and variable intensity compared to the low temperature solid. This area may contain a minor solid-state phase transition *circa* -56°C . (b) Detail of cryogenic temperature solid state vibrational modes with relative intensities scaled for this region as in Fig. 3a. Note spectral details in the low frequency ($200\text{--}350\text{ cm}^{-1}$) range.

$\text{C}10=\text{C}11$ double bond. The groups $\text{C}8\text{--}\text{C}9$ and $\text{C}12\text{--}\text{C}13$ produce torsion in the same direction relative to the $\text{C}10=\text{C}11$ plane, *i.e.* DPA bending. Since the $\text{C}10=\text{C}11$ bond is the central double bond, $\text{C}7=\text{C}8$ and $\text{C}13=\text{C}14$ will both be either above or below the $\text{C}10=\text{C}11$ plane.

Alternatively, when torsion is in the opposite direction ($\text{C}11\text{--}\text{C}12\text{--}\text{C}13=\text{C}14$ at -95° and $\text{C}13=\text{C}14\text{--}\text{C}15\text{--}\text{C}16$ at $+90^{\circ}$), *i.e.* DHA, torsion manifests instead as a twist at the central $\text{C}13=\text{C}14$ bond; additionally $\text{C}11\text{--}\text{C}12$ and $\text{C}15\text{--}\text{C}16$ are on opposite sides of the $\text{C}13=\text{C}14$ plane. This relative direction of torsion enables distinguishing sites where localized torsion is nonzero. A temperature gradient adds torque at sites of torsion, and a redistribution of thermal energy (relaxation of thermal stress) minimizes the net impact of the torsion increase. Since in any $\text{C}_n=\text{C}_{n+1}$ structure, torsion and torque can be different at C_n vs. C_{n+1} , torsion redistribution between C_n and C_{n+1} sites also need not be equal (Ogurtani, 2006, 2016).

Overall our results describe *n*-6DPA as a roughly planar three-dimensional structure. However, DHA, with no noticeable CH_2 bending but CH_2 twisting, is best described as a flat helical structure with small pitch due to a similar direction of torsion/twist among the six double bonds. This structure is good agreement with models which hypothesize DHA fitting into the rhodopsin α -helix (Feller et al., 2003; Kachlishvili and Brenna 2013). It also independently confirms nuclear magnetic resonance and fluorescence decay results (Eldho et al., 2003; Mitchell et al., 2012) which concluded that DHA within the lipid bilayer is

oriented more parallel to the membrane surface than perpendicular, as is commonly depicted. We believe we have presented independent spectroscopic evidence to corroborate hypotheses in which DHA-containing lipids can interweave with helical proteins

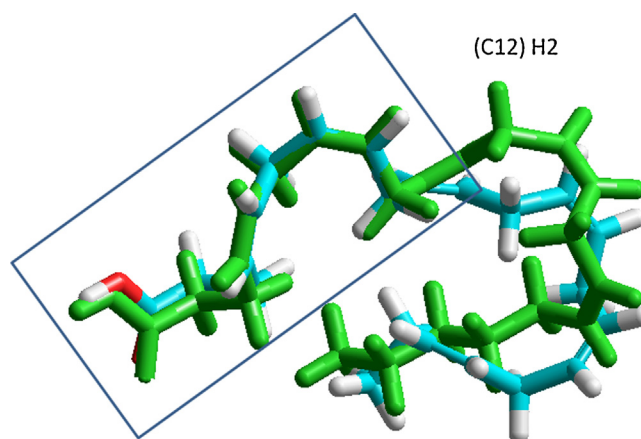


Fig. 6. Overlay of energy minimized solid state structures of DHA (carbon blue, hydrogen white, oxygen red) and *n*-6 DPA (all green). From $\text{C}1$ to $\text{C}11$ conformation is almost identical; then DHA shifts to a more helical structure. (For interpretation of the references to colour in this figure legend, the reader is referred to the web version of this article.)

Table 2a

C–C–C–C dihedral angles.

Molecular Site	DHA Dihedral Angle (°)		DPA Dihedral Angle (°)		Shift from DHA to DPA (°)	
–C3H ₂ –						
C2–C3–C4 C5		–116		–101		15
C3–C4 C5–C6	–0.7		0.6		1.3	
–C6H ₂ –						
C4 C5–C6–C7	91		140		49	
C5–C6–C7 C8		121		119		–2
C6–C7 C8–C9	–0.8		–0.6		0.2	
–C9H ₂ –						
C7 C8–C9–C10	78		80		2	
C8–C9–C10 C11		–140		–148		–8
C9–C10 C11–C12	–0.5		–0.5		0.0	
–C12H ₂ –						
C10 C11–C12–C13	–169		–157		12	
C11–C12–C13 C14		–103		–95		8
C12–C13 C14–C15	–0.1		–0.2		–0.1	
–C15H ₂ –						
C13 C14–C15–C16	117		90		–27	
C14–C15–C16 C17		–112		–125		–13
C15–C16 C17–C18	0.6		0.1		–0.5	
–C18H ₂ –						
C16 C17–C18–C19	–92		–99		–7	
C17–C18–C19=C20		–119				
C18–C19=C20–C21	–0.5					
–C21H ₂ –						
C19=C20–C21–C22	90					

Torsion angles in DHA and DPA are obtained from the lowest energy [and predominantly planar] structures of each generated using HyperChem. Torsion can be measured toward the carbonyl carbon C1 or towards the methyl carbon C22. Torsion angles are only reported for four atom sets that contain a double bond. In all C_nC_{n+1} sites, C–C–C_nC_{n+1} torsion angles do not equal C_nC_{n+1}–C–C torsion angles. Torsion for C–C_nC_{n+1}–C was less than 1° out of plane. Sites of C–C–C–C torsion are reasonably similar between DHA and DPA.

Table 2b

H–C–C dihedral angles.

Molecular Site	DHA Dihedral Angle (°)		DPA Dihedral Angle (°)		Shift from DHA to DPA (°)	
DB 1						
H _a –C3–C4 C5	126		139		13	
H _b –C3–C4 C5	5		21		16	
C4 C5–C6–H _a		–147		–98		49
C4 C5–C6–H _b		–29		21		50
DB 2						
H _a –C6–C7 C8	–117		–120		–3	
H _b –C6–C7 C8	10		–1		–9	
C7 C8–C9–H _a		–163		–161		2
C7 C8–C9–H _b		–45		–42		3
DB 3						
H _a –C9–C10 C11	101		93		–8	
H _b –C9–C10 C11	–17		–26		–9	
C10 C11–C12–H _a		68		–80		–148
C10 C11–C12–H _b		–51		–39		12
DB 4						
H _a –C12–C13 C14	131		144		13	
H _b –C12–C13 C14	13		26		13	
C13 C14–C15–H _a		–125		–154		–29
C13 C14–C15–H _b		–7		–37		–30
DB 5						
H _a –C15–C16 C17	130		–98		228	
H _b –C15–C16 C17	13		22		9	
C16 C17–C18–H _a		146		117		–30
C16 C17–C18–H _b		23		–2		–25
DB 6						
H _a –C18–C19 C20	120					
H _b –C18–C19 C20	1					
C19 C20–C21–H _a		–150				
C19 C20–C21–H _b		–32				

Torsion angles in DHA and DPA are obtained from the lowest energy [and predominantly planar] structures of each generated using HyperChem. The four moieties C=C–CH_a, C=C–CH_b, H_aC–C=C, and H_bC–C=C each have discretely different torsion angles. At any one CH₂ site, torsion angles of H_a and H_b are very different. DHA and DPA are most dissimilar at C12H₂.

to form stable but highly dynamic three-dimensional structures with extended π bond interaction.

Raman vibrational modes that occur during the phase transitions are properties of a major fraction of the 22 carbon chain fatty acid. Torsion is present over six atoms in the sequence $H_a-C-C=C-C-H_a$, (relative to $H_b-C-C=C-C-H_b$) due to increase the curvature from H_a to the next H_a . Specific sequences of $H_a-C-C=C-C-H_a$ can individually have greater torsion. Changes in elasticity can occur unequally as a function of the temperature gradient among the $C_n=C_{n+1}$ plus $C_{n-1}H_2$ and $C_{n+2}H_2$ sites. Interestingly, in specific temperature ranges, CH_2 rocking can shift to $H-CC=C$ or $C=CC-H$ wagging: every $(HC=CH)-CH_2-(HC=CH)$ site includes the possibility of $H-CC=C$ or $C=CC-H$ wagging occurring at a given temperature. The precise structures of all LC-PUFA of interest over longer molecular distances and within the lipid bilayer are still to be deciphered. However, *a priori* limiting the molecular dimensions for vibrational modes overlooks longer molecular sequences which can contain very stable torsion. This in turn precludes understanding curvature, torsion and torque components that cause anisotropy in PUFA.

Conflict of interest

None.

References

- Akanbi, T.O., Sinclair, A.J., Barrow, C.J., 2014. Pancreatic lipase selectively hydrolyses DPA over EPA and DHA due to location of double bonds in the fatty acid rather than regioselectivity. *Food Chem.* 160, 61–66.
- Brenna, J.T., Carlson, S.E., 2014. Docosahexaenoic acid and human brain development: evidence that a dietary supply is needed for optimal development. *J. Hum. Evol.* 77, 99–106.
- Broadhurst, C.L., Schmidt, W.F., Kim, M.S., Nguyen, J.K., Qin, J., Chao, K., Gary, L., Bauchan, G.L., Shelton, D.R., 2015. Continuous gradient temperature Raman spectroscopy of oleic and linoleic acids from -100 to 50°C . *Proceedings SPIE (International Society for Photonics and Optics)*, Baltimore, MD, 21–22 April 2015 (also submitted for publication to *Lipids*, 2016).
- Byelashov, O.A., Sinclair, A.J., Kaur, G., 2015. Dietary sources, current intakes, and nutritional role of omega-3 docosapentaenoic acid. *Lipid Technol.* 27, 79–82.
- Chen, J., Jiang, Y., Liang, Y., Tian, X., Peng, C., Ma, K.Y., Liu, J., Huang, Y., Chen, Z.Y., 2012. DPA n-3, DPA n-6 and DHA improve lipoprotein profiles and aortic function in hamsters fed a high cholesterol diet. *Atherosclerosis* 221, 397–404.
- Crawford, M.A., Broadhurst, C.L., Guest, M., Nagar, A., Wang, Y., Ghebremeskel, K., Schmidt, W.F., 2013. A quantum theory for the irreplaceable role of docosahexaenoic acid in neural cell signalling throughout evolution. *Prostaglandins Leukot. Essent. Fat. Acids* 88, 5–13.
- Crawford, M.A., Broadhurst, C.L., Cunnane, S., Marsh, D.E., Schmidt, W.F., Brand, A., Ghebremeskel, K., 2014. Nutritional armor in evolution: docosahexaenoic acid as a determinant of neural, evolution and hominid brain development. *Mil. Med.* 179 (Suppl. 11), 61–75.
- Dyall, S.C., Michael-Titus, A.T., 2008. Neurological benefits of omega-3 fatty acids. *Neuromol. Med.* 10, 219–235.
- Dyall, S.C., 2015. Long chain omega-3 fatty acids and the brain: a review of the independent and shared effects of EPA, DPA and DHA. *Front. Aging Neurosci.* 7, 1–15.
- Eldho, N.V., Feller, S.E., Tristram-Nagle, S., Polozov, I.V., Gawrisch, K., 2003. Polyunsaturated docosahexaenoic vs. docosapentaenoic acid—differences in lipid matrix properties from the loss of one double bond. *J. Am. Chem. Soc.* 125, 6409–6421.
- Feller, S.E., Gawrisch, K., Woolf, T.B., 2003. Rhodopsin exhibits a preference for solvation by polyunsaturated docosohexaenoic acid. *J. Am. Chem. Soc.* 125, 4434–4435.
- Gawrisch, K., Soubias, O., 2008. Structure and dynamics of polyunsaturated hydrocarbon chains in lipid bilayers—significance for GPCR function. *Chem. Phys. Lipids* 153, 64–67.
- Hamam, F., Shahidi, F., 2006. Synthesis of structured lipids containing medium-chain and omega-3 fatty acids. *J. Agric. Food Chem.* 54, 4390–4396.
- Janssen, C.I., Kiliaan, A.J., 2014. Long-chain polyunsaturated fatty acids (LCPUFA) from genesis to senescence: the influence of LCPUFA on neural development aging, and neurodegeneration. *Prog. Lipid Res.* 53, 1–17.
- Kachlishvili, K., Brenna, T.J., 2013. Steric effects in the interaction between transmembrane proteins and polyunsaturated phospholipids. *J. Biol. Phys. Chem.* 13, 36–44.
- Kaur, G., Cameron-Smith, D., Garg, M., Sinclair, A.J., 2011. Docosapentaenoic acid (22:5n-3): a review of its biological effects. *Prog. Lipid Res.* 50, 28–34.
- Lewis, R.N., McElhane, R.N., 2013. Membrane lipid phase transitions and phase organization studied by Fourier transform infrared spectroscopy. *Biochim. Biophys. Acta* 1828, 2347–2358.
- Mishra, S., Chaturvedi, D., Kumar, N., Tandon, P., Siesler, H.W., 2010. An *ab initio* and DFT study of structure and vibrational spectra of γ form of oleic acid: comparison to experimental data. *Chem. Phys. Lipids* 207, 163.
- Mitchell, D.C., Niu, S.-L., Litman, B.J., 2012. Quantifying the differential effects of DHA and DPA on the early events in visual signal transduction. *Chem. Phys. Lipids* 165, 393–400.
- Moriguchi, T., Lim, S.-Y., Greiner, R., Lefkowitz, W., Loewke, J., Hoshiba, J., Salem Jr., N., 2004. Effects of an n-3-deficient diet on brain, retina, and liver fatty acyl composition in artificially reared rats. *J. Lipid Res.* 45, 1437–1445.
- Nauroth, J.M., Liu, Y.C., Van Elswyk, M., Bell, R., Hall, E.B., Chung, G., Arterburn, L.M., 2010. Docosahexaenoic acid (DHA) and docosapentaenoic acid (DPA n-6) algal oils reduce inflammatory mediators in human peripheral mononuclear cells in vitro and paw edema in vivo. *Lipids* 45, 375–384.
- Niu, S.L., Mitchell, D.C., Lim, S.Y., Wen, Z.M., Kim, H., Salem, N., Litman, B.J., 2004. Reduced G protein-coupled signaling efficiency in retinal rod outer segments in response to n-3 fatty acid deficiency. *J. Biol. Chem.* 279, 31098–31104.
- Ogurtani, T.O., 2006. Unified theory of linear instability of anisotropic surfaces and interfaces under capillary, electrostatic and elastostatic forces: the regrowth of epitaxial amorphous silicon. *Phys. Rev. B* 74, 1–25.
- Ogurtani, T.O., 2016. Curvature, torsion and torque in helical conformations and the stability and growth of α -peptides under isochoic and isobaric conditions. *Phys. Rev. B* doi:<http://dx.doi.org/10.13140/RG.2.1.1431.3041> (Personal Communication) (submitted for publication).
- Pi, F., Kaneko, F., Iwahashi, M., Suzuki, M., Ozaki, Y., 2011. Solid-state low temperature \rightarrow middle temperature phase transition of linoleic acid studied by FTIR spectroscopy. *J. Phys. Chem. B* 115, 6289–6295.
- Qin, J., Chao, K., Kim, M.S., 2010. Raman chemical imaging system for food safety and quality inspection. *Trans. Am. Soc. Agric. Biol. Eng.* 53, 1873–1882.
- SanGiovanni, J.P., Chew, E.Y., 2005. The role of omega-3 long-chain polyunsaturated fatty acids in health and disease of the retina. *Prog. Retin. Eye Res.* 24, 87–138.
- Schmidt, W.F., Broadhurst, C.L., Qin, J., Li, H., Nguyen, J.K., Chao, K., Hapeman, C.J., Shelton, D.R., Kim, M.S., 2015a. Continuous temperature-dependent Raman spectroscopy of melamine and structural analog detection in milk powder. *Appl. Spectrosc.* 69, 398–406.
- Schmidt, W.F., Kim, M.S., Nguyen, J.K., Qin, J., Chao, K., Broadhurst, C.L., Shelton, D.R., 2015b. Continous gradient temperature Raman spectroscopy identifies flexible sites in proline and alanine peptides. *Vib. Spectrosc.* 80, 59–65.
- Schultz, Z., 2011. Raman spectroscopic imaging of cholesterol and docosahexaenoic acid in the retinal rod outer segment. *Aust. J. Chem.* 64, 611–616.
- Skulas-Ray, A.C., Flock, M.R., Richter, C.K., Harris, W.S., West, S.G., Kris-Etherton, P.A., 2015. Red blood cell docosapentaenoic acid (DPA n-3) is inversely associated with triglycerides and c-reactive protein (CRP) in healthy adults and dose-dependently increases following n-3 fatty acid supplementation. *Nutrients* 7, 6390–6404.
- Ueno, A., Miyazaki, A., Yano, J., Furukawa, Y., Suzuki, M., Sato, K., 2000. Polymorphism of linoleic acid (*cis*-9,*cis*-12-octadecadienoic acid) and α -linoleic acid (*cis*-9,*cis*-12,*cis*-15-octadecatrienoic acid). *Chem. Phys. Lipids* 107, 169–178.
- Unger, M., Chaturvedi, D., Mishra, S., Tandon, P., Siesler, H.W., 2013. Two-dimensional correlation analysis of temperature-dependent FT-IR spectra of oleic acid. *Spectrosc. Lett.* 46, 21–27.